Optimal Sensor Location in Motion Control of Flexibly Supported Long Reach Manipulators

Constantinos Mavroidis, Steven Dubowsky and Kevin Thomas
Department of Mechanical Engineering
Massachusetts Institute of Technology, Cambridge, MA 02139
Tel.: (617)-253-2144, Fax: (617)-258-7881, e-mail: dubowsky@mit.edu

Keywords: Optimal Sensor Placement, Flexible Manipulators, End-Point Control

Abstract

Long reach manipulator systems (LRMS) are robotic systems that are used to perform important tasks in difficult to reach locations such as space or nuclear environment. They consist of a relatively small and fast manipulator mounted on a long-reach flexible structure that can exhibit substantial vibrations when the manipulator performs its task. The Inferred End-Point Control (IEC) is a method that has been proposed to control the position and orientation of long reach manipulators in spite of their supporting structure vibrations. In this method the manipulator's end-effector position and orientation in inertial space is "inferred" by strain measurements on the flexible structure. In this paper the important problems of determining the minimum number of strain sensors needed and their optimal placement on the flexible supporting structure of LRMS are addressed. A methodology to optimally place the strain sensors on the flexible structure is developed. The selection criteria in this method are: high measurement resolution, maximum distance from singular locations and minimum error in the identification of the structure's strain-displacement model. This method for optimally placing strain sensors is validated with simulations and experiments using a six degree of freedom laboratory long reach manipulator system called Shaky II. Using the optimally selected strain locations, it is shown that with IEC the manipulator end-effector position/orientation can accurately be controlled in spite of the structure’s vibrations.

1. INTRODUCTION

Long reach manipulator systems (LRMS) are a special class of robotic systems that are used to perform important tasks in difficult to reach locations. They consist of a relatively small and fast manipulator mounted on a larger, long-reach, deployable, flexible structure. The repair of high voltage power transmission towers and lines, the inspection of underground storage tanks, the repair of bridges and space systems maintenance (see Figure 1) are some of the applications where LRMS are used [1-3].

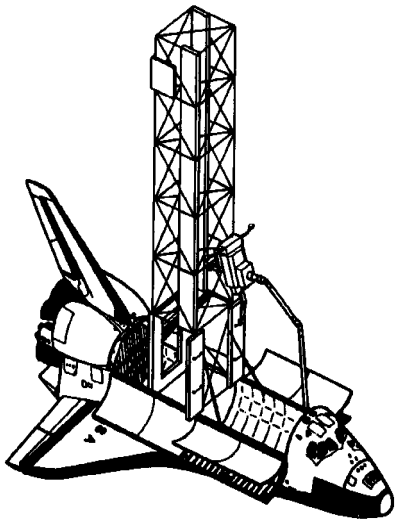

Figure 1: Maintenance of space systems using LRMS

A key problem that the designer of LRMS has to face is that external disturbances such as wind or impacts with the environment and the motion of the system itself can excite low frequency, lightly damped vibrations of the manipulator deployable supporting structure. These vibrations would make the system difficult to control, corrupt the measurements and endanger the system with impacts on the site.

Research has been done to reduce the effects of the supporting structure vibrations on the performance of long reach manipulators [4]. A path-planning method has been developed, called the Coupling Map method, that finds paths for the small dexterous manipulator that minimize the vibrational energy transferred to its deployable structure during a space task [5]. Bracing methods

have been suggested to increase the system stiffness in some general applications of long reach systems [6]. Control methods have been proposed and are distinguished in two classes: damping control and end-point control. Methods of the first class aim to damp out the deployable structure's vibrations using the small manipulator controller [7-9]. In end-point control, the position and orientation in inertial space of the end-effector of the small manipulator, is controlled in spite of the supporting structure vibrations [10-15]. End-point control is a very promising way to control LRMS in real applications since the manipulator stays near the task location and it does not need to interrupt its task operation to damp out its supporting structure's vibrations.

In end-point control the manipulator end-effector position and orientation needs to be measured in an inertial reference system. In most of the methods proposed to date, the end-effector position and orientation feedback comes by either direct measurements of the position/orientation of the manipulator end-effector [10-12] or by direct measurements of the position/orientation of a reference system defined at the mounting point of the manipulator on its structure and then using the manipulator kinematics to deduce the end-effector position/orientation [13, 14]. These measurements are performed by sensors that do not take into account the physical properties of the system but have the ability to give inertial position and orientation information for a reference system defined at a specific point on the system. Sensors that have been used are lasers, cameras, gyroscopes, ultrasonic sensors. These sensors have limitations. They have limited range, their ability to measure the position/orientation of the end-effector is limited by the presence of obstacles, they may need additional hardware and design considerations or they may need the placement of targets. Clearly, the use of these sensors in remote, hostile, and partially known environments such as in space and nuclear environment is very difficult.

Indirect methods to measure the position of the manipulator end-effector or the mounting point of the manipulator on its structure have been proposed. These methods that combine sensor information and model based techniques are using the internal physical properties of the structure and do not present the limitations that direct methods have such as need for good knowledge of the

environment. One of the indirect methods consists of obtaining measurements of the interaction forces and moments between the manipulator and its flexible structure and then from dynamic simulations using a finite element model of the structure calculate its motion [15]. The identification of the dynamic parameters of the structure and the computation burden are important issues that need to be considered with this method.

Another indirect method of measuring the position/orientation of the manipulator is called Inferred End-Point Control (IEC) [16]. In this method, from easily obtained strain measurements on the flexible structure and a simple static model of the structure its motion is estimated. Then using the small manipulator's kinematic model, the position/orientation of the end-effector is obtained in an inertial reference system. An additional advantage of IEC to the advantages that indirect methods have is its low computational requirements.

In this paper the important problems of determining the minimum number of strain sensors needed and their optimal placement on the flexible supporting structure of LRMS so that the performance of IEC is improved, are addressed. Solutions to these problems will facilitate the practical implementation of IEC in real applications of LRMS.

Optimal sensor location is a common problem in many engineering applications. It is important in cases where the properties of a system described as continuous functions need to be identified using discrete sensor information from the system. From practical point of view, it is impossible to have infinite number of sensor measurements on the structure and the problem is stated as: "what is the minimum number of sensors needed and what is the optimal location of these sensors on the system to best approximate the system's properties?" This problem is very often addressed when dealing with flexible mechanical systems [17-19]. In robotics it has been studied in perception and tactile sensing applications [20-21]. This problem is formulated as an optimization problem where a performance criterion is optimized over a finite set of possible sensor locations.

In this paper, the optimal location of strain sensors on the flexible supporting structure of LRMS is obtained using the following performance criteria:

i) high measurement resolution of the structure's motion
ii) maximum distance from "singular" locations
iii) minimum error in the identification of the structure's strain-displacement model

Finite element theory, linear algebra, singular value decomposition and sensitivity analysis of linear systems are used to find the optimal strain locations. The effectiveness of the method is validated in simulations and experimentally using a prototype laboratory six degree of freedom LRMS called Shaky II. Using the optimally selected strain locations, it is shown that with IEC the manipulator end-effector position/orientation can accurately be controlled in spite of the structure's vibrations.

2. KINEMATIC EQUATIONS

2.1 Notation

Consider a general long reach, flexible based manipulator such as the manipulator shown in Figure 2. A deployable, reconfigurable, lightly damped flexible structure is fixed at one end in inertial space (point I in Figure 2) and at the other end (point B on the figure) supports a small, dexterous, rigid body m-joint manipulator. At points I and B two reference systems R_i and R_b are defined. When the manipulator system is at rest, the two reference systems have their axes parallel and the position of B in R_i is defined by the geometrical properties of the supporting structure. When the manipulator moves and the flexible structure vibrates, R_b moves with the structure's free end. The position of R_b with respect to R_i, is represented by the 3 by 1 position vector of B in R_i: ${}^i\mathbf{r}_B=[x_b, y_b, z_b]^T$, and the orientation of R_b with respect to R_i by a 3x3 rotation matrix ${}^i\mathbf{A}_b(\varphi)$ composed of the three euler angles written in vector form as $\varphi=[\varphi_x, \varphi_y, \varphi_z]^T$. A third reference system, R_e, is defined at point E, the manipulator end-point. Its position and orientation with respect to R_i is defined by the 3 by 1 position vector of E in R_i: ${}^i\mathbf{r}_E=[x_e, y_e, z_e]^T$, and the 3x3 rotation matrix ${}^i\mathbf{A}_e(\theta)$ composed of the three euler angles $\theta=[\theta_x, \theta_y, \theta_z]^T$.

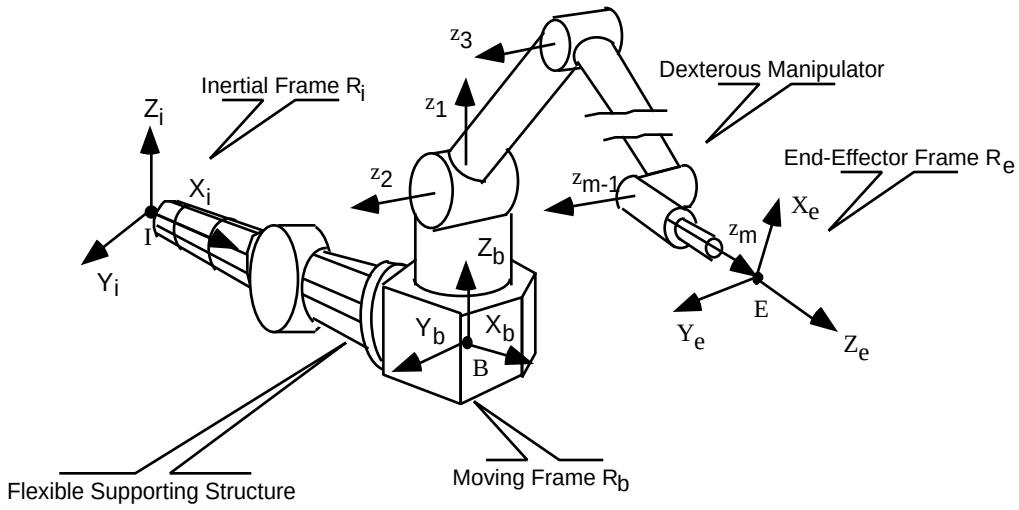

Figure 2: Schematic of a general long reach manipulator system

2.2 Manipulator Position Kinematics

For the system shown in Figure 2 the following kinematic equations describe its end-effector inertial position and orientation:

$$
\begin{aligned}
{}^{i}\mathbf{r}_E &= {}^{i}\mathbf{A}_b(\varphi)\,{}^{b}\mathbf{r}_e(\mathbf{q}) + {}^{i}\mathbf{r}_B \\
{}^{i}\mathbf{A}_e(\theta) &= {}^{i}\mathbf{A}_b(\varphi)\,{}^{b}\mathbf{A}_e(\mathbf{q})
\end{aligned}
\tag{1}
$$

where ${}^{b}\mathbf{r}_E=[{}^{b}x_e,\ {}^{b}y_e,\ {}^{b}z_e]^T$ is the position vector of E in R_b and ${}^{b}\mathbf{A}_e$ is the orientation of E in R_b. ${}^{b}\mathbf{r}_E$ and ${}^{b}\mathbf{A}_e$ are functions of the rigid manipulator joint variables grouped here in a vector $\mathbf{q}=[q_1, q_2,\ldots, q_m]^T$. From equation (1) it is obvious that if the manipulator joint variables $\mathbf{q}$ and the position and orientation of R_b with respect to R_i (i.e. the vectors ${}^{i}\mathbf{r}_B$ and φ) are known then the position and orientation of R_e in inertial reference system can be calculated. The manipulator joint variables $\mathbf{q}$ are easily measured with joint position sensors such as encoders. Different methods have also been proposed to measure ${}^{i}\mathbf{r}_B$ and φ [13, 14, 16]. In this work, strain measurements on the deployment structure are used to measure ${}^{i}\mathbf{r}_B$ and φ. This method will be described in the next section.

2.3 Supporting Structure's Static Linear Strain-Displacement Model

The problem that is being studied here is how to obtain the displacement parameters of reference systems defined at certain locations on a flexible structure from a number of strain measurements on the structure. In ideal situations where very simple structures are used such as homogeneous, symmetrical, one dimensional flexible systems it is possible to obtain analytically this model. However in real applications, the flexible structures are very complex systems and no analytical calculation of the strain-displacement model can be performed. Here, finite elements analysis of structures will be used to obtain the model that relates strains in certain locations of the structure and the displacement parameters of certain reference systems on the structure. Small displacement, static analysis and linear elastic structures are assumed.

Consider a finite element model of a flexible structure. It is assumed that the finite element model is very close to reality which means that the number of nodes, k, is very large. From finite element theory [e.g. 22], it can be shown that:

$$\boldsymbol{\varepsilon} = \mathbf{B}\ \mathbf{u} \tag{2}$$

where $\mathbf{u}$ is a 6k x 1 vector containing all the nodal motion parameters (it is assumed that each node has six degrees of freedom), $\boldsymbol{\varepsilon}$ is a 6l x 1 vector containing the strain parameters at l distinct locations on the structure (it is assumed that at each location six strains are developed) and $\mathbf{B}$ is a 6l x 6k coefficient matrix whose elements depend on the geometry of the finite element model, and more specifically on the coordinates of the nodes and the coordinates of the strain locations. Equation (2) is called the "strain-displacement" equation and its physical meaning is that if the nodal displacements are known then the strains at any location on the structure can be obtained. All vectors $\mathbf{u}$ form a vector space of dimension 6k called the "displacement space" of the structure and will be represented by the letter U. All vectors $\boldsymbol{\varepsilon}$ form a vector space of dimension 6l called the "strain space" of the structure and will be represented by the letter E. Equation (2) represents

the linear mapping of U into E. Since the numbers k and l are large, with no loss of generality they can be selected to be equal and this mapping can be inverted. Then equation (2) is written as:

$$\mathbf{u} = \mathbf{B}^{-1} \varepsilon \tag{3}$$

Equations (2) and (3) describe a one to one mapping between the two spaces under the assumptions: (i) the number of nodes k and the number of strain locations l are very big so that the continuous functions describing the structure's displacement field and the structure's strain field are closely approximated by the discrete spaces spanned by **u** and ε, (ii) the spaces E and U are of the same dimension, i.e. matrix B is square and non-singular.

In the problem considered in this paper, the displacement parameters of only few of the nodes of the system's flexible supporting structure need to be known. For example, for the system shown on Figure 3 which is a schematic of a two manipulator long reach system, the motion parameters of points A and B which are the mounting points of the two manipulators on the structure need to be known. In general, if the motion parameters of n nodes of the system need to be known with n less than k, the 6nx1 vector $\mathbf{u}_m$ of the node motion parameters is calculated by the following equation:

$$\mathbf{u}_m = \mathbf{S}\ \mathbf{B}^{-1}\ \varepsilon = \mathbf{A}\ \varepsilon \tag{4}$$

where **S** is a 6n x 6k selection matrix. Matrix **A** is a 6n x 6l scaling matrix, that depend on the geometry of the structure and the local coordinates of nodes and strain locations. All vectors $\mathbf{u_m}$ form a subspace of U that will be called the "reduced displacement space" and will be represented by the vector U_m.

While the mapping between the spaces E and U described by Equation (3) is one to one, the mapping between the subspace U_m. and E is not one to one. Consider for example the flexible structure shown on Figure 4. This structure under two different loading conditions maintains the same inertial position and orientation for a reference system defined at point A. Using Equation (3)

for each loading configuration there is a different strain vector ε of E mapped into a displacement vector $\mathbf{u}$ of U (Note: the motion parameters of A are just some of the coordinates of $\mathbf{u}$).

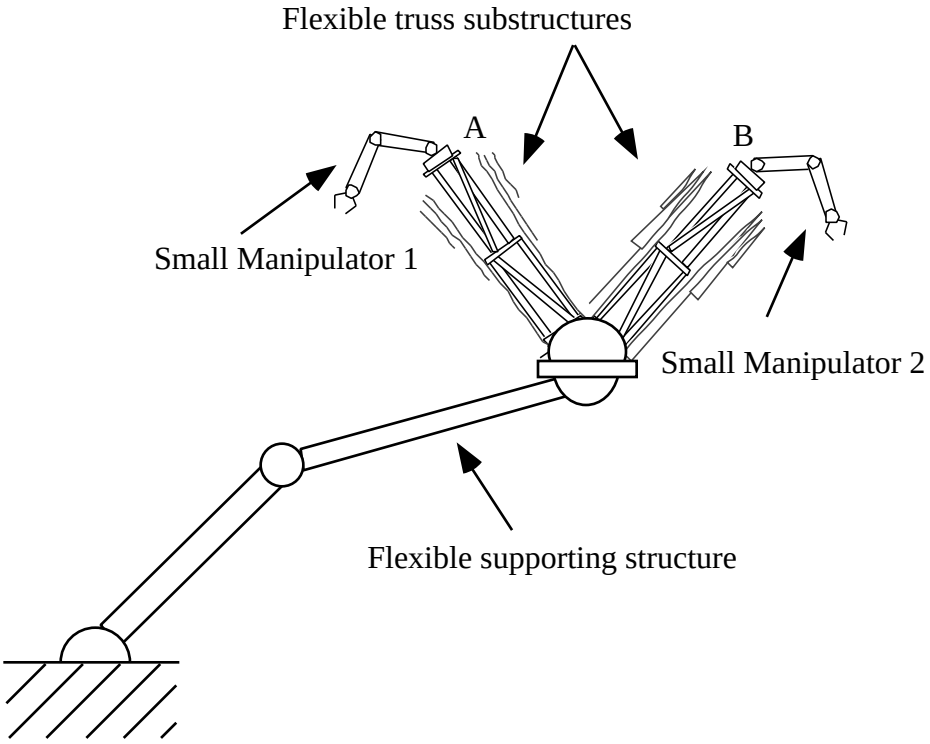

Figure 3: Schematic of a complex two manipulator long reach system

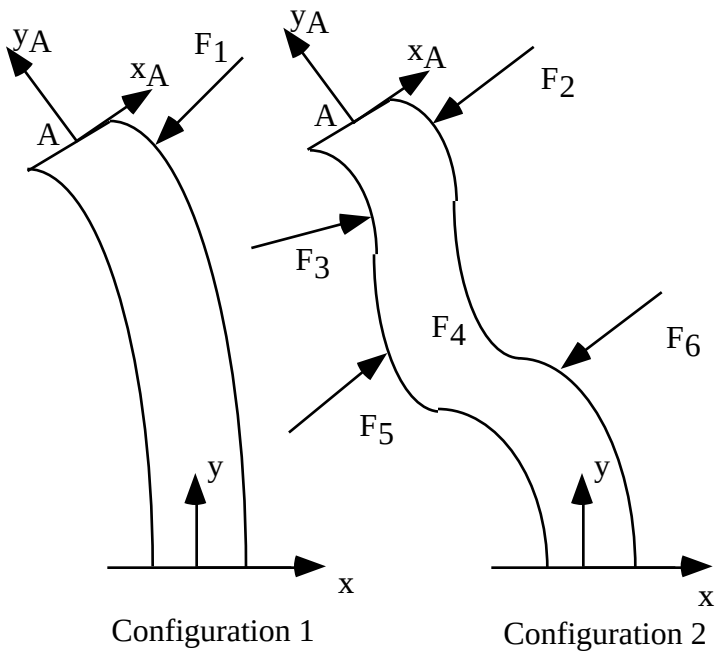

Figure 4: Same displacement of point A with two different loading conditions

However, if the space U_m is defined by the vector $\mathbf{u_m}$ of the motion parameters of node A then for each loading configuration there is a different vector ε of space E but both vectors are mapped into the same vector $\mathbf{u_m}$ of U_m. Therefore two vectors ε of space E may have the same image in U_m. Two vectors in U_m. are always the images of two different vectors in E. While the two strains vectors ε have the same image in U_m however they represent two different "modes" of deformation of the structure. If the system is constrained to move under the same mode, for example as in configuration 1, then each vector $\mathbf{u_m}$ of U_m is the image of only one strain vector ε and the mapping between spaces U_m and E becomes one to one.

3 OPTIMAL SELECTION OF STRAIN SENSOR LOCATION

3.1 Minimum Number of Strain Sensors

If all motion parameters of the n nodes studied are independent then the dimension of U_m is 6n. This means that there are 6n independent vectors $\mathbf{u}_m^{\mathbf{i}}$ (i=1..6n) that form a basis of U_m . These vectors represent fundamental displacements of the n nodes of the system and all other displacement vectors $\mathbf{u}_m$ are a linear combination of $\mathbf{u}_m^{\mathbf{i}}$. Each vector $\mathbf{u}_m^{\mathbf{i}}$ is the image of one vector $\varepsilon^{\mathbf{i}}$ that belong in E provided that the system always moves in the same mode (see section 2.3). Each vector $\mathbf{u}_m^{\mathbf{i}}$ and its corresponding vector $\varepsilon^{\mathbf{i}}$ can be the ith column of a 6nx6n matrix $\mathbf{U_m}$ and of a 6lx6n matrix **E** respectively. Matrix $\mathbf{U_m}$ is called the "reduced displacement matrix" and matrix **E** will be called the "strain matrix". From Equation (4) the following equation is obtained:

$$\mathbf{U}_m = \mathbf{A}\ \mathbf{E} \tag{5}$$

Since the columns of $\mathbf{U_m}$ are independent then the columns of **E** are also independent (if not then there is a vector in E that has two images in U_m). The column space of **E** has dimension 6n. From linear algebra, it is known that the dimension of the column space of a matrix is equal to its row space [23]. Therefore only 6n rows of the 6l of **E** are independent and equation (5) takes the form:

$$\mathbf{U}_m = \mathbf{A}_m \ \mathbf{E}_m \tag{6}$$

where $\mathbf{E_m}$ is a 6nx6n submatrix of **E** called "the reduced strain matrix" and $\mathbf{A_m}$ is a 6nx6n scaling matrix. The columns of $\mathbf{E_m}$ are the basis of a subspace of E of dimension 6n called the "reduced strain space" and will be represented by the letter E_m.

The physical meaning of the existence of a subspace E_m of E of dimension 6n so that each vector $\boldsymbol{\varepsilon}_\mathbf{m}$ of E_m. has an image in U_m and vice versa, is that from the original 6l strains measured on the structure, 6n strains can be found to estimate the displacement parameters of n nodes on the structure. If a vector $\boldsymbol{\varepsilon}_\mathbf{m}$ of E_m. is given then its corresponding vector $\mathbf{u_m}$ in U_m is found from the following equation:

$$\mathbf{u}_m = \mathbf{A}_m . \boldsymbol{\varepsilon}_m \tag{7}$$

3.2 Optimal Sensor Locations

A search procedure has been established to find the "best" location of 6n measurements among all possible combinations from the initial 6l.

3.2.1 Criteria for optimal selection:

Three criteria have been set to select the best location on the structure of the strain sensors. These criteria are:

(i) higher measurement resolution

This criterion satisfies two needs. First, to be able to measure very small displacements the strain sensors should be located in areas of higher strain resolution when the nodes are displaced a minimum amount of distance from their nominal position. In this case, there are locations on the structure where the strains developed are less than the minimum value that the strain sensor can detect. Obviously these locations should be excluded from further consideration. A typical lower

limit of the measurement capabilities of strain sensors is 10^{-6} and a typical value of displacement measurement resolution is 0.5-1mm for the translations and 0.05-0.1 degrees for the rotations. The second reason why this criterion is important is that it reduces rapidly the dimension of the search space. The number 6l of all possible strain location is very big. With this criterion that acts like a filter, a first reduction of the high dimension strain space is achieved. This is important in the next steps where computationally heavy search algorithms are applied.

(ii) higher "distance" from singularity

The problem of finding the "best" location for 6n strain measurement on the structure is equivalent to the problem of finding the "best" 6nx6n submatrix $\mathbf{E_m}$ of $\mathbf{E}$. Matrix $\mathbf{E_m}$ of Equation (6) can be any 6nx6n submatrix of $\mathbf{E}$ with rank equal to 6n. It is known from linear algebra and the theory of matrix computations [24] that the rank of a matrix is equal to the number of its non-zero singular values. Using the singular value decomposition, the reduced strain matrix $\mathbf{E_m}$ is written as:

$$\mathbf{E_m} = \mathbf{W}.\Sigma.\mathbf{V}^{\mathbf{T}} \tag{8}$$

where $\mathbf{W}$ and $\mathbf{V}$ are 6nx6n orthogonal matrices and Σ is a 6nx6n diagonal matrix. The columns of $\mathbf{W}$ and $\mathbf{V}$ are the left and right singular vectors of $\mathbf{E_m}$.The elements of the first diagonal of Σ are the singular values of matrix $\mathbf{E_m}$ written in descendent order:

$$\Sigma = \begin{bmatrix} \sigma_{max} & 0 & \cdots & 0 \\ 0 & \ddots & & \vdots \\ \vdots & & \ddots & 0 \\ 0 & \cdots & 0 & \sigma_{min} \end{bmatrix} \tag{9}$$

The minimum singular value σ_{min} is important because it represents the measure of how far matrix $\mathbf{E_m}$ is from matrices of lower rank [25]. If all singular values are not equal to zero (i.e. $\sigma_{min}>0$) then the rank of matrix $\mathbf{E_m}$ is 6n. If r singular values are equal to zero (i.e. at least $\sigma_{min}=0$), then the rank of matrix $\mathbf{E_m}$ is equal to 6n-r. This means that the dimension of the reduced strain space E_m is 6n-r and its image space in the displacement space U through Equation (6) is a subspace of U_m. In this case it is not possible to obtain the values of the motion parameters of the n nodes that

are studied with these 6n strain measurements and these strain measurements are not admissible. In strain locations where σ_{min} is not zero but has a value close to zero, matrix $\mathbf{E_m}$ is said to be “close to singularity" and "near rank deficiency". This situation needs also to be avoided since it is related with errors and increased sensitivity to small perturbations in the system's parameters.

Therefore the best $\mathbf{E_m}$ from all 6nx6n submatrices of $\mathbf{E}$ is the one with the maximum σ_{min}.

(iii) <u>better identification of matrix A_m</u>

Elements of matrix $\mathbf{A_m}$ are identified writing Equations (6) as:

$$\mathbf{A}_m = \mathbf{U}_m \ \mathbf{E}_m^{-1} \tag{10}$$

It is known, from the theory of sensitivity analysis of linear systems [26], that if matrix $\mathbf{E_m}$ is "ill-conditioned" small errors in the elements of matrix $\mathbf{E_m}$ induce big errors in the identification of matrix $\mathbf{A_m}$. The condition number c of $\mathbf{E_m}$ gives a measure of how much errors in $\mathbf{E_m}$ may be magnified in the computed solution and is defined as:

$$c = \|\mathbf{E}_m\| \ \|\mathbf{E}_m^{-1}\| \tag{11}$$

If $\delta\mathbf{A_m}$ is the error in the calculation of $\mathbf{A_m}$ due to an error $\delta\mathbf{E_m}$ of $\mathbf{E_m}$ then the following inequality exists:

$$\frac{\|\delta\mathbf{A}_m\|}{\|\mathbf{A}_m\|} \le c \ \frac{\|\delta\mathbf{E}_m\|}{\|\mathbf{E}_m\|} \tag{12}$$

If c is close to 1 then matrix $\mathbf{E_m}$ is said to be "well-conditioned" and the error $\delta\mathbf{A_m}$ is small.

The error $\delta\mathbf{u_m}$ in the measurement of $\mathbf{u_m}$ due to an error $\delta\mathbf{A_m}$ of matrix $\mathbf{A_m}$ and due to strain measurement errors $\delta\boldsymbol{\varepsilon}_\mathbf{m}$ is equal to:

$$\delta\mathbf{u}_m = \mathbf{A}_m \ \delta\boldsymbol{\varepsilon}_m + \delta\mathbf{A}_m \ \boldsymbol{\varepsilon}_m + \delta\mathbf{A}_m \ \delta\boldsymbol{\varepsilon}_m \tag{13}$$

The error $\delta\mathbf{u_m}$ becomes minimal when $\delta\mathbf{A_m}$ is very small. Therefore it is important to select a matrix $\mathbf{E_m}$ with a low condition number.

Usually if σ_{min} of matrix $\mathbf{E_m}$ has a large value, as it is found from criterion (ii), then matrix $\mathbf{E_m}$ has a good condition number c and criterion (iii) may seem redundant. However there are structures for which although σ_{min} is maximized for all possible strain locations on the structure, it has a small value. Then criterion (iii) becomes an important constraint in the search procedure.

It is important to note that since the elements of matrix **E** are dimensionless, criteria (ii) and (iii) do not depend on change of unit, scale, or reference system.

3.2.2. Algorithm Development

Using the above criteria a search method has been established to find the best strain measurement locations on the flexible structure. First a finite element model of the structure is made. The number of nodes k and the number of strain measurement locations l is defined. The number of degrees of freedom per node and the number of strains per location is determined (for this section it is assumed that 6 degrees of freedom per node and 6 strains per strain locations are developed.) n nodes are selected for which the motion parameters will be calculated. The displacement matrix $\mathbf{U_m}$ representing the fundamental displacements for the n nodes is defined. For each fundamental displacement, static simulations from the finite element model are performed and the 6nx6l strain matrix **E** is found. A desired resolution is defined for each of the n nodes and using criterion (i), p strain measurement locations are selected (with $p<6l$) that present higher strain resolution. These p locations correspond to p rows of the **E** matrix. A new 6nxp strain matrix **E'** is formed.

Then using criteria (ii) and (iii) the "best" 6nx6n submatrix $\mathbf{E_m}$ of **E'** is found. The obvious way to find the best $\mathbf{E_m}$ is to form all 6nx6n submatrices of **E'**, calculate its σ_{min} and select the submatrix with the higher σ_{min}. However, this method is computationally very expensive. Consider for example, the simple case where only one node is studied (n=1) with 6 degrees of

freedom and that after filtering with criterion (i) there are 100 possible strain measurements (p=100.) Then the dimensions of matrix $\mathbf{E}'$ are 100x6 and there are 10^9 6x6 submatrices of $\mathbf{E}'$. The computation of the best $\mathbf{E_m}$ with this way can take days. The algorithm used in this work requires only few computations. The first 6n-1 rows of $\mathbf{E_m}$ are set to be equal to the first 6n-1 rows of $\mathbf{E}'$ and for the last row of $\mathbf{E_m}$ all possibilities are tried. With this way the number of 6nx6n matrices that are formed reduces considerably. For the same example used above, now there are only 100 $\mathbf{E_m}$ matrices to form. The row for which $\mathbf{E_m}$ has the larger σ_{min} while it condition number is smaller than a pre-specified value, is found and becomes the first row of $\mathbf{E_m}$. Then the same exhaustive search is repeated for the last row and the new "best row becomes the second row of $\mathbf{E_m}$ and so on. It turns out that this algorithm converges to an optimal solution very fast.

The various steps of this search procedure are shown schematically on Figure 5. On the figure, in some of the steps explanatory comments are shown written in Matlab language [27].

The strain displacement linear model (Equation 7) that was used to optimally place the strain sensors on the flexible structures and estimate the displacement of certain nodes on the structure is configuration dependent. If the structure is deployable, as for example in the case of long reach manipulators, and is being deployed into a new configuration, for each configuration a new model needs to be calculated. In this work it is assumed that the flexible deployable supporting structure of LRMS, is deployed in one configuration and then locked at this configuration.

In the rest of the paper it is assumed that the motion parameters of only one node on the structure need to be known (n=1).

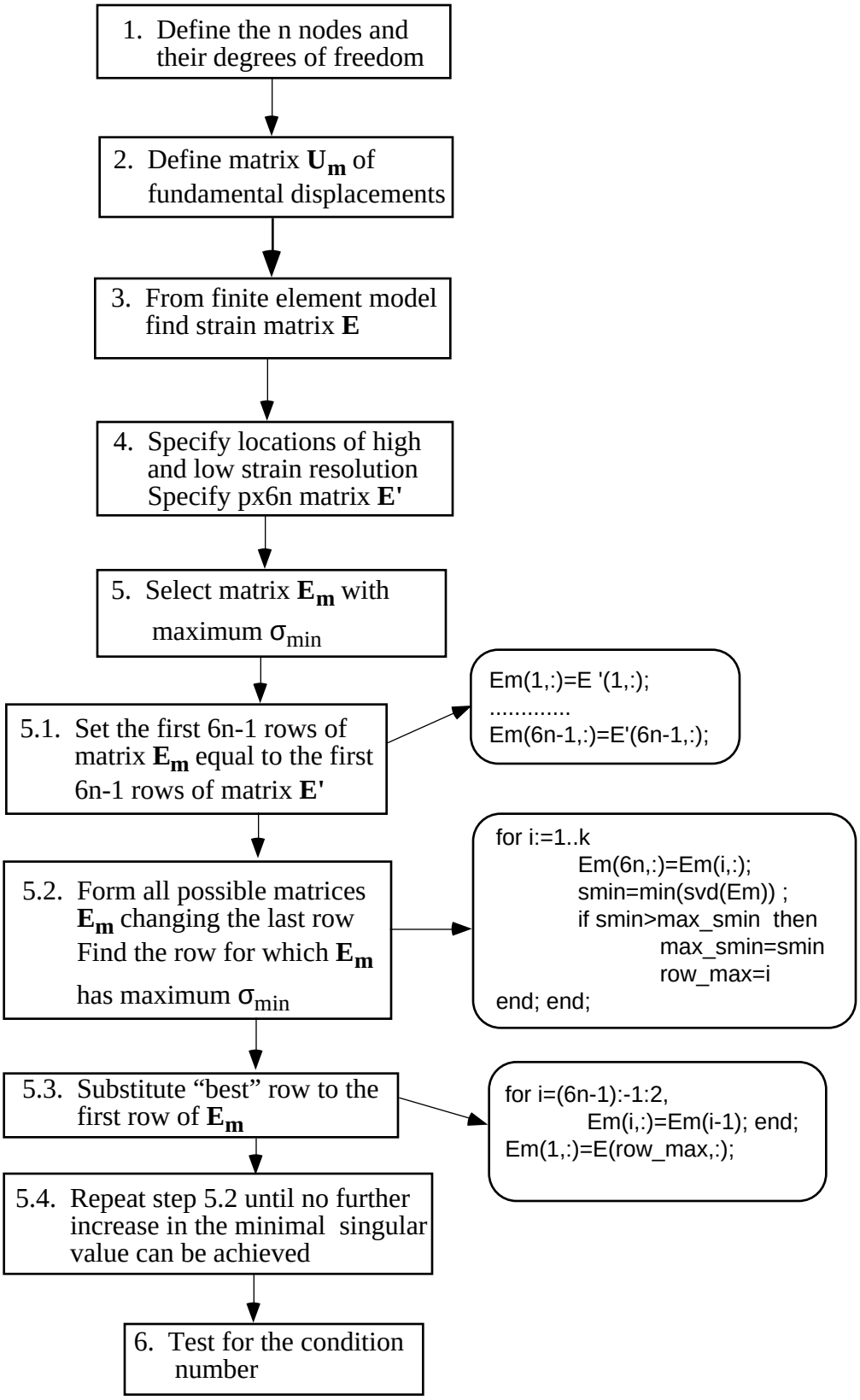

Figure 5: Search algorithm for optimal strain placement

4 INFERRED ENDPOINT CONTROL

The linear relationship between strains on the supporting structure of a LRMS and displacement of the reference system defined at the mounting point of the manipulator on the structure is used to estimate the position and orientation of the manipulator end-effector in an inertial reference system. This is equivalent to a manipulator end-point sensing technique by measuring the strains on the supporting structure. This end-point sensing technique has been used in [16] in an end-point controller that is called Inferred End-Point Control (IEC). In this section a summary of the Inferred End-Point Control is presented.

The proposed Inferred End-Point Control for long reach manipulator systems is based on cartesian based controllers widely developed to control the end-effector positions of conventional fixed-base manipulators. These controllers are designed so that virtual forces and moments are exerted at the manipulator's end-effector [28-30]. Classically, the virtual forces and moments are simple functions of the cartesian space end-effector position and velocity errors, such as:

$$\mathbf{F} = \mathbf{K}_p \mathbf{e} + \mathbf{K}_d \dot{\mathbf{e}} = \mathbf{K}_p(\mathbf{X}_d - \mathbf{X}) + \mathbf{K}_d(\dot{\mathbf{X}}_d - \dot{\mathbf{X}}) \tag{14}$$

where: $\mathbf{F}$ is the vector of virtual forces and moments at the manipulator end-effector. $\mathbf{X}$ and $\dot{\mathbf{X}}$ are the vectors of the inertial end-effector position/orientation and velocity. $\mathbf{X}_d$ and $\dot{\mathbf{X}}_d$ are the vectors of the desired inertial end-effector position/orientation and velocity. $\mathbf{e}$ and $\dot{\mathbf{e}}$ are the vectors of the inertial end-effector position and velocity errors. $\mathbf{K}_p$ and $\mathbf{K}_d$ are the position and velocity control gain matrices. Assuming a LRMS such as the one in Figure 2 and using the terminology introduced in section 2, $\mathbf{X}=[{}^i\mathbf{r}_E, \theta]^T$. $\mathbf{X}$ is calculated from Equation (1) using encoder measurements of the manipulator joint angles $\mathbf{q}$ and estimates of the manipulator base position and orientation Ψ with $\Psi=[{}^i\mathbf{r}_B, \varphi]^T$ (see section 2). Ψ is calculated from strain measurements on the structure using Equation (7) (here Ψ is the vector $\mathbf{u}_m$ of Equation (7)) The endpoint velocity $\dot{\mathbf{X}}$ is obtained from a numerical derivation procedure on $\mathbf{X}$. Comparing the values of $\mathbf{X}$ and $\dot{\mathbf{X}}$ to the desired $\mathbf{X}_d$ and $\dot{\mathbf{X}}_d$, provides the error signals for the operational space controller.

The manipulator joint torques and the induced manipulator/supporting structure interaction forces are calculated from the virtual forces and moments using equation (14):

$$\tau = \begin{pmatrix} \tau_m \\ \mathbf{F}_I \end{pmatrix} = \mathbf{J}^T\mathbf{F} = \begin{pmatrix} \mathbf{J}_m & \mathbf{J}_b \end{pmatrix}^T \mathbf{F} \tag{15}$$

where: τ is the vector of the joint torques and manipulator/structure interaction forces and moments, τ_m is the vector of the manipulator joint torques, $\mathbf{F}_I$ is the vector of the manipulator base/structure interaction forces and moments, $\mathbf{J}$ is the augmented Jacobian matrix of the long reach manipulator in R_i, $\mathbf{J}_m$ is the Jacobian matrix of the fixed base manipulator in R_i, $\mathbf{J}_b$ is the Jacobian matrix that transforms reference system's R_b linear and angular velocities into manipulator end-point velocities.

This augmented form of Equation (15) is similar to the one developed for free-flying space robotic systems and manipulators mounted on mobile suspension vehicles [31, 32]. As with these systems , the augmented manipulator Jacobian has the form:

$$\mathbf{J} = \begin{pmatrix} \mathbf{J}_m & \mathbf{J}_b \end{pmatrix} = \begin{pmatrix} \mathbf{A}(\varphi) & 0 \\ 0 & \mathbf{A}(\varphi) \end{pmatrix} \mathbf{J}_{fb}(\mathbf{q}) \begin{pmatrix} \mathbf{I} & -\mathbf{A}(\varphi)\mathbf{B}(\mathbf{q})\mathbf{A}^T(\varphi) \\ 0 & \mathbf{I} \end{pmatrix} \tag{16}$$

where: $\mathbf{J}_{fb}$ is the conventional nxm Jacobian matrix of the fixed base manipulator in R_b $\mathbf{q}$ is the mx1 vector of the manipulator joint angles $\mathbf{B}(\mathbf{q})$ has the form:

$$\mathbf{B}(\mathbf{q}) = \begin{pmatrix} 0 & -z_e^b & y_e^b \\ z_e^b & 0 & -x_e^b \\ -y_e^b & x_e^b & 0 \end{pmatrix} \tag{17}$$

The manipulator torques τ_m, given Equation (15), will result in a manipulator motion that will tend to drive $\mathbf{X}$ to $\mathbf{X}_d$. Since the interaction forces and moments $\mathbf{F}_I$ are not controllable, but determined by the characteristics of the deployment structure, they will act as disturbances to the system. They will, in general, result in some manipulator base motion and some end-effector errors that must be compensated for, by the manipulator joint actions [32].

A block diagram of the Inferred End-Point Control algorithm is shown in Figure 6.

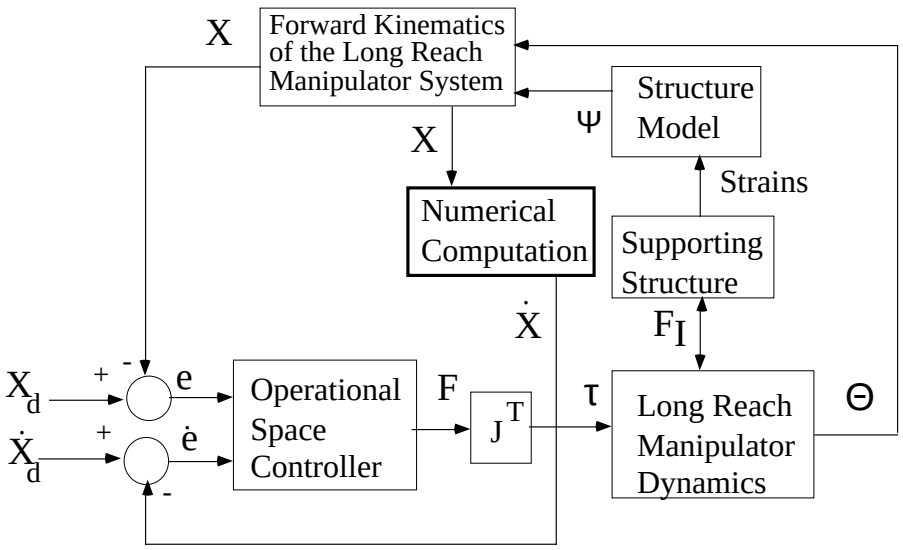

Figure 6: Inferred End-Point Control algorithm for Long Reach Manipulators

5. METHOD EVALUATION

5.1 Experimental System

An experimental laboratory LRMS, called Shaky II, has been built to validate the method for optimally placing the strain sensors on the flexible structure of LRMS to better estimate its motion. Experimental results show that the manipulator end-effector inertial position/orientation measurement is better when the optimally selected strain locations are used. Performance of the Inferred Endpoint Control using the optimal strain locations is presented.

Shaky II consists of a 5 foot vertical flexible member that supports a PUMA 250 (see Figure 7.) The supporting structure is a 3.5 inch (8.89 cm) outer diameter and 0.3125 inch (0.79 cm) wall thickness, sculptured, non-metallic, PolyVinyl Chloride tube. It has six levels of diamond shaped holes at its lower end, each level staggered 60˚ compared to the previous one. This pattern of holes make the tube very flexible and lightly damped. It was designed to give to the structure spatial motion characteristics close to those of real LRMS. Due to these holes the structure's shape is complex so that analytical methods can not be applied. On Figure 8 a close view of the hole pattern and the system's dimensions are given.

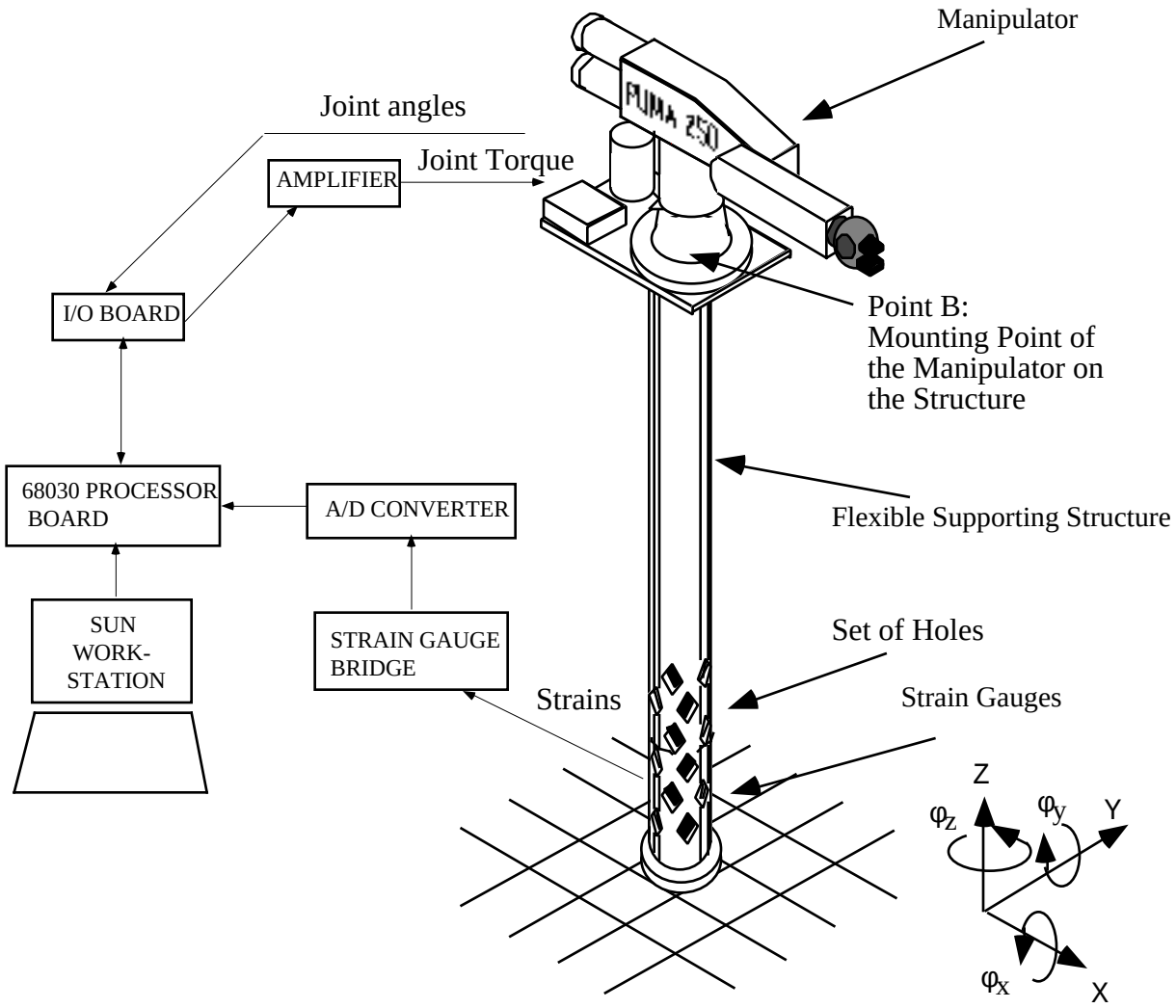

Figure 7: Schematic of the MIT Spatial LRMS - Shaky II

The structure's stiffness matrix was found to be:

$$\mathbf{K} = \begin{bmatrix} 678\ \text{N/m} & 0 & 0 & 0 & 603\ \text{N/rad} & 0 \\ 0 & 644\ \text{N/m} & 0 & -556\ \text{N/rad} & 0 & 0 \\ 0 & 0 & 7.10^{5}\ \text{N/m} & 0 & 0 & 0 \\ 0 & -556\ \text{N} & 0 & 683\ \text{Nm/rad} & 0 & 0 \\ 603\ \text{N} & 0 & 0 & 0 & 593\ \text{Nm/rad} & 0 \\ 0 & 0 & 0 & 0 & 0 & 2.10^{3}\ \text{Nm/rad} \end{bmatrix} \quad (18)$$

From this stiffness matrix it is obvious that there is no rotation and translation around the Z axis (see Figure 7). The reference system defined at point B, the manipulator mounting point on the structure, has four degrees of freedom: translation and rotation around the X and Y axes. The

amplitude of linear motion along both axes is ±8 cm and of rotational motion is 2-3˚. The natural frequency of motion is approximately 0.9 Hz in each direction.

Shaky's II manipulator is a PUMA 250 manipulator. It is a 3-link, 6 degree-of-freedom robotic manipulator. For this work only the first three joints were considered. It weighs 25 pounds (11 kg) and has a maximum reach of 25.5 inches (65 cm).

This experimental set-up is controlled by a 32-bit Motorola 68030 microprocessor single board computer running at 20 MHz. VxWorks is used as a real-time operating system.

The complete description and design of the system can be found in [33].

5.2. Finite Element Analysis

A finite element model was built for Shaky's II supporting structure using the finite element analysis program ADINA [34]. On Figure 8 a detailed description of the various elements used, the position of nodes on each element and some of the strain measurement locations are shown.

The model consists of five pipe elements and 18 shell elements. Each pipe element has two nodes, 16 strain measurement locations with 5 strains developed at each strain location (it is assumed that for the pipe element there is no torsion)and a total of 80 strains measured. The shell element has 8 nodes, 18 strain measurement locations (there are two layers where strains are measured, 9 locations per level, see Figure 8) with 6 strains developed per location and a total of 108 strains measured. In total the finite element model has 85 nodes and 2344 strains are measured.

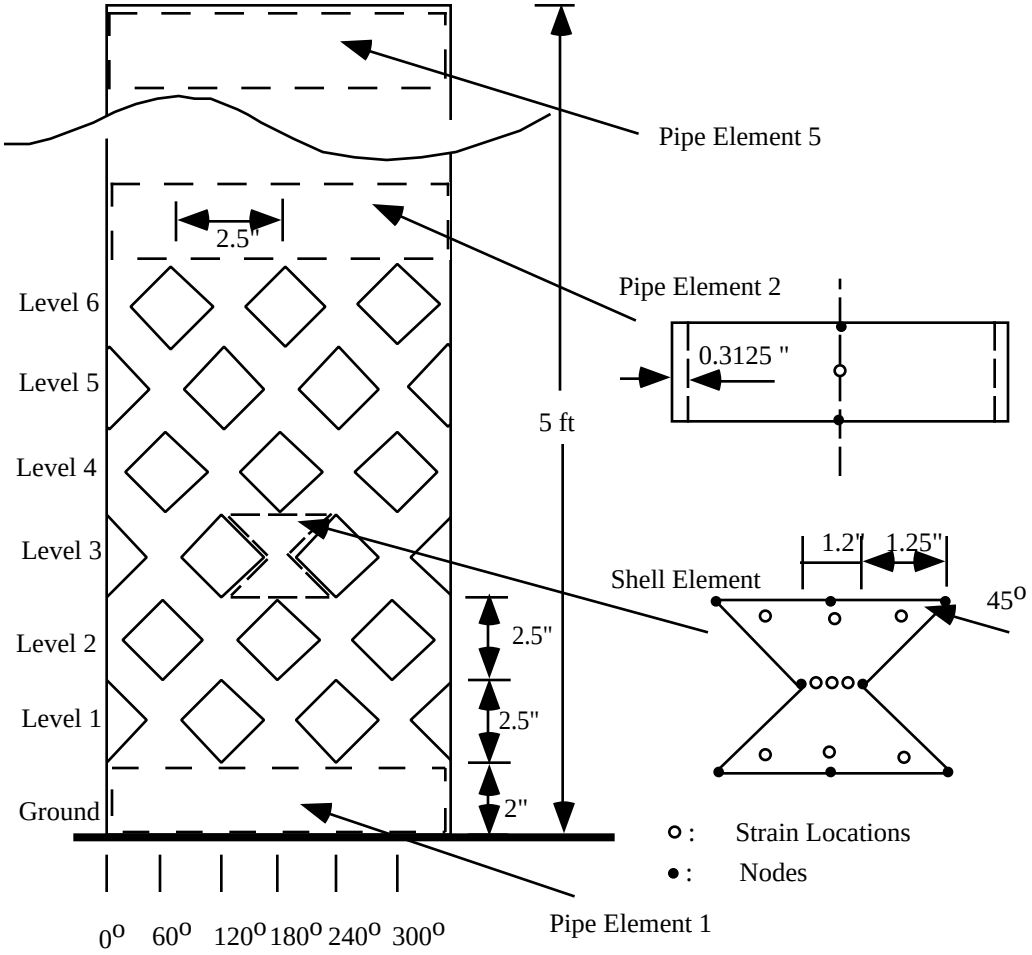

Figure 8: Detailed schematic of the hole pattern

The displacement parameters of only one node need to be known (n=1), the mounting point of the manipulator on its supporting structure, point B of Figure 7. As discussed above, the reference system defined at this point has four degrees of freedom: translation along axes X and Y and rotation around the same axes. Therefore the dimension of vector space U_m is equal to 4. This means that only 4 strain measurements should be performed. Each vector $\mathbf{u}_m$ that belong in this space has the form $\mathbf{u}_m=[x_b, y_b, \varphi_x, \varphi_y]^T$ with x_b, y_b, φ_x, φ_y, the motion parameters of node B. The matrix $\mathbf{U}_m$ of fundamental displacements was found to be:

$$\mathbf{U}_m = \begin{bmatrix} 0.01 & 0 & 0 & 0.011 \\ 0 & 0.01 & -0.011 & 0 \\ 0 & -0.008 & 0.01 & 0 \\ 0.008 & 0 & 0 & 0.01 \end{bmatrix} \qquad (19)$$

Each column of $\mathbf{U}_m$ represents an independent displacement of B and the four columns are a basis of U_m . Any other displacement of B is a linear combination of these four fundamental displacements (with the assumption of small displacements.) The first column, for example, means that there is 0.01 m translation along X and a rotation 0.008 rad around Y. The definition of each fundamental displacement should take into account the motion characteristics of the structure such as the motion coupling.

The strain matrix **E** is formed running simulations of the finite element model using as input each one of the fundamental displacements. The dimensions of **E** are 2344 x 4. A first reduction in the dimension of the strain space is to assume that strains can be measured only on the external surface of the structure. In this way the dimension of **E** become 1172 x 4. Using criterion (i) it was found that high stain resolution area contains the 18 shells elements and the pipe elements 1 and 2 which are immediately attached to the shell elements (see Figure 8.) Then matrix **E'** is formed with dimensions 1052 x 4. Using criteria (ii) and (iii) and the search algorithm described on Figure 5, the 4x4 submatrix $\mathbf{E_m}$ of **E'** with maximum minimal singular value and with a good condition number was estimated. The rows of $\mathbf{E_m}$ correspond to one strain measurement on the structure.

On Figure 9, three different sets of four strain locations are shown which will be called as: "location 1", "location 2" and "location 3". At each location on the shell elements six strains are developed that are represented with the vector $\varepsilon=[\varepsilon_x, \varepsilon_y, \varepsilon_z, \varepsilon_{xy}, \varepsilon_{xz}, \varepsilon_{zy}]^T$. On the figure, at each strain location, it is also shown which coordinate of the vector ε is measured.

Location 1 is the "best" and it corresponds to the best $\mathbf{E_m}$ found using the methodology described in section 3. The minimal singular value of $\mathbf{E_m}$ is $\sigma_{min} = 0.32 \cdot 10^{-4}$ and its condition number c=25. Location 2 is the best under the assumption that at each location only the axial strain ε_z and the circumferencial strain ε_{xy} can be measured. This assumption simplifies the experimental implementation. For this location $\sigma_{min} = 0.15 \cdot 10^{-4}$ and its condition number c=31. This location was also found using the method of section 3. Location 3 is a "bad" location that was chosen

arbitrarily. For this location $\sigma_{min} = 0.013 \cdot 10^{-4}$ and c=176, values that are worse than in the other two locations.

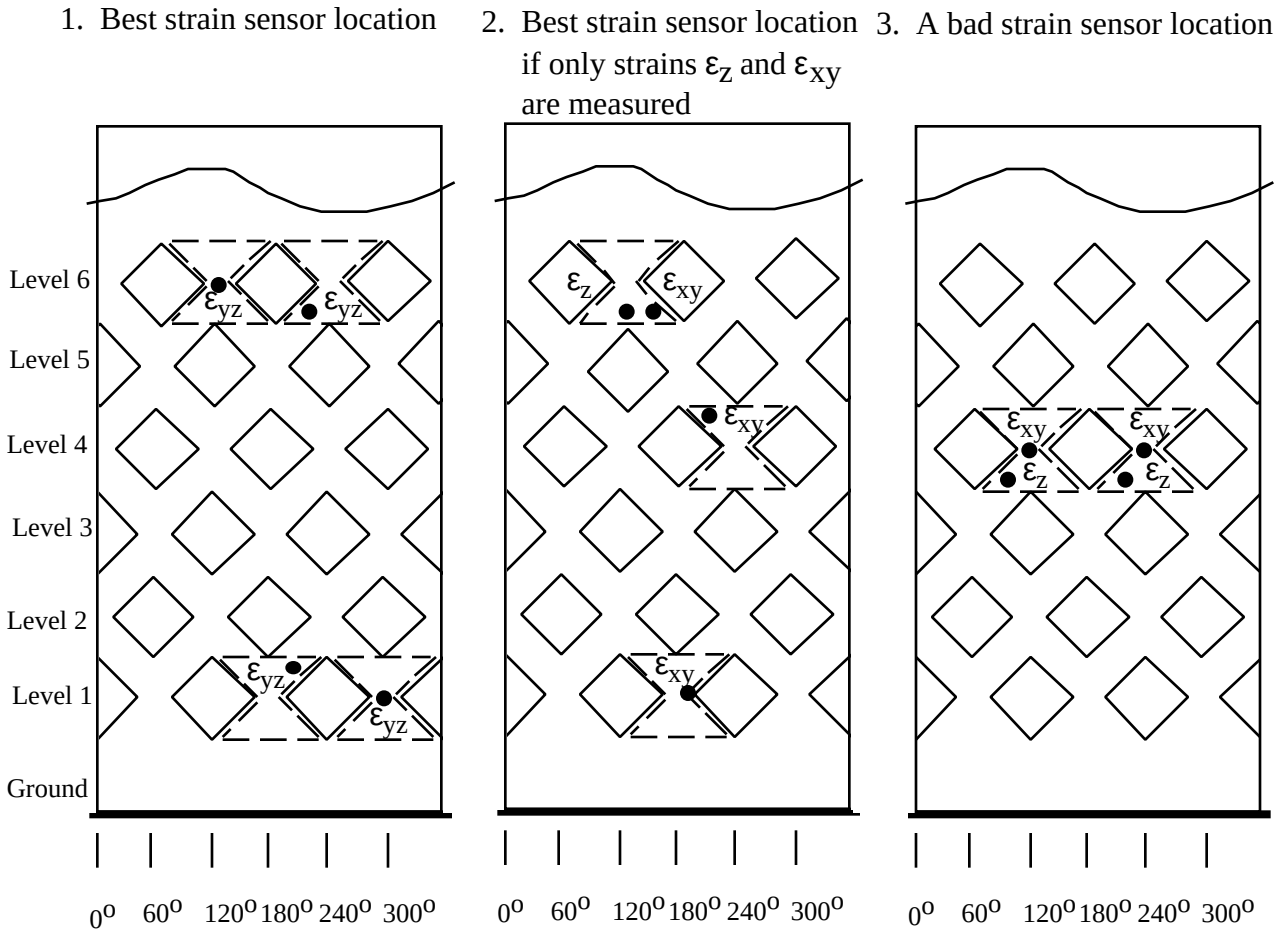

Figure 9: Two "good" strain sensor locations and one "bad"

To demonstrate the effectiveness of our method an error is introduced in the model parameters. It is assumed that the real wall thickness of the tube is equal to 0.3464" (0.88cm) instead of 0.3125" (0.79 cm) that was used to find the optimal location of strain gauges and to calculate matrix $\mathbf{A_m}$ of Equation (7).. We want to see how robust is the estimation of the displacements of point B with Equation (7) if the identification of matrix $\mathbf{A_m}$ was done using a 10% error in one of the model parameters, for each of three strain locations shown on Figure 9. This error in one of the model parameters changes the strains developed along the structure and is equivalent as introducing errors

in the strain measurements. Therefore the robustness of our displacement estimate using Equation (7) is also tested in the presence of errors in the strain measurement.

Using the finite element model and the altered value of the wall thickness, three known displacements $\mathbf{u_1}$=[1cm, 1cm, -0.45˚, 0.45˚]^T, $\mathbf{u_2}$=[2cm, 2cm, -0.91˚, 0.91˚]^T and $\mathbf{u_3}$=[3cm, 3cm, -1.37˚, 1.37˚]^T are imposed at point B. For each displacement the strains are calculated along the structure. Among the strains those that corresponds to locations 1 to 3 of Figure 9 are selected. For each strain location, using the corresponding strains and the corresponding matrix $\mathbf{A_m}$ that was calculated with the old value of the wall thickness, through Equation 7 three estimates of the displacements $\hat{\mathbf{u}}_1$, $\hat{\mathbf{u}}_2$ and $\hat{\mathbf{u}}_3$ are calculated. For each location these estimates are compared to the original displacements. On Figure 10 the results from these tests are shown.

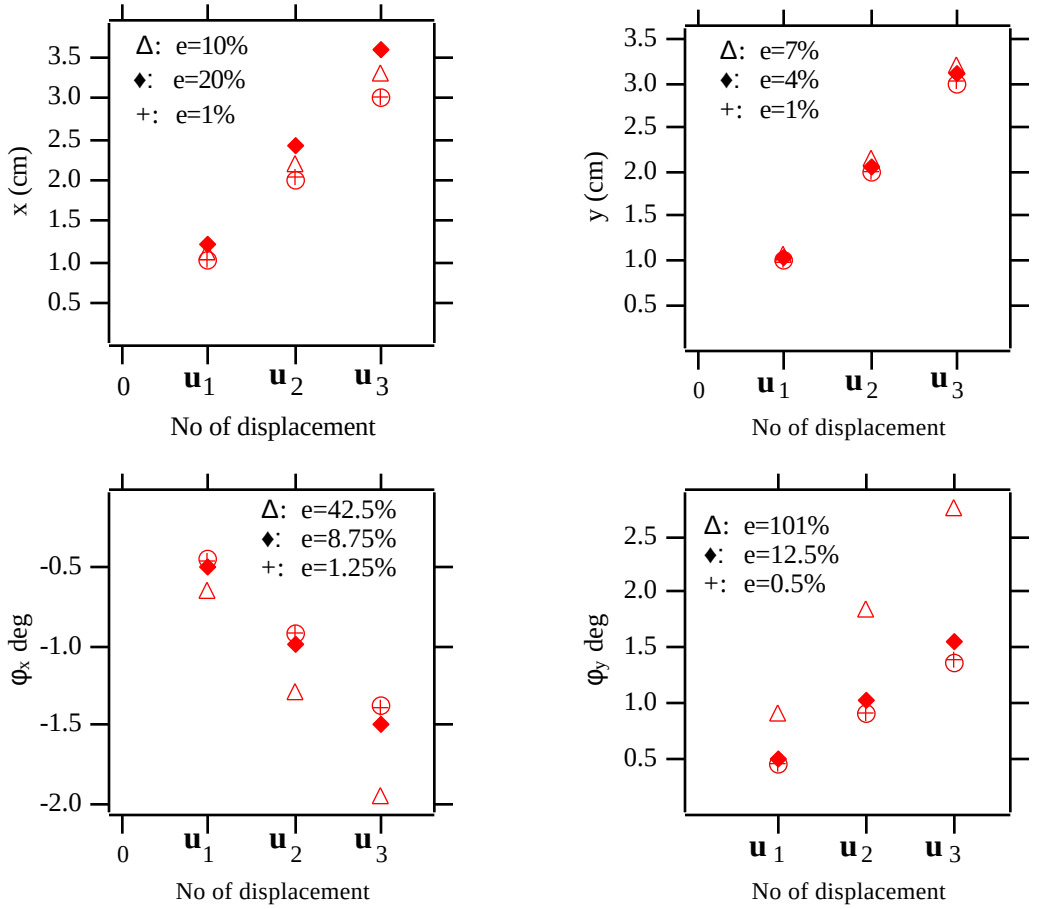

Figure 10: Simulation tests of displacement estimation

Each diagram on Figure 10 corresponds to one of the four coordinates of the three displacements . The real values of the coordinates of each displacement is represented by a circle. The estimates of the coordinates of the displacements using strains on location 1 are marked with a "+", using strains on location 2 with a "♦" and using strains on location 3 with "Δ". The maximum percentage of error e in the estimation of the displacement is also shown.

From Figure 10 it is clear that the estimates obatined with the strains on location 1 are the best with an average error in all directions of 0.9% in spite of the error in the model parameters. Estimates of the displacements using the strains on location 2 also give good results with an average error of 11.3%. Strains on location 3 lead to bad estimates of the displacements especially for rotations. The estimates of the displacement using these strains have an average error of 40%.

5.3. Experimental Results

Experiments were done using Shaky II. The goal of these experiments was: (i) to verify that strain measurements obtained in a "good" location based on our methodology of section 3.2 give better estimates of the structure's motion than those located in a "bad" location, and (ii) to validate experimentally IEC on Shaky II using as end-effector position feed-back estimates obtained from Equation (1) using as strain measurements those in the "good" position.

5.3.1 Measurement of the structure's motion

Shaky II's structure is displaced manually in the same three positions $\mathbf{u_1}$, $\mathbf{u_2}$ and $\mathbf{u_3}$ of the reference system defined at point B, (see Figure 7) as in the simulation tests. In each displacement of the structure, strain measurements are obtained that correspond to locations 2 and 3 defined on Figure 9. (To simplify experiments no strains from location 1 are obtained.) As the methodology in section 3.2 suggested and as the simulation results verified strain measurements at location 2 are "good" while those at location 3 are "bad". Using Equation (7) estimates of displacements $\mathbf{u_1}$, $\mathbf{u_2}$ and $\mathbf{u_3}$ are obtained. For each set of strain measurements, matrix $\mathbf{A_m}$ of Equation (7) is calculated experimentally using a calibration procedure described in [33]. The results from these tests are

shown on Figure 11. The same notation is used as in Figure 10. It is clear that the estimates obtained with the strains measured in location 2 are much better than those of location 3. The average error in all directions in the displacement estimates using the strains in location 2 is 11% while the average error using the strains in location 3 is 19%.

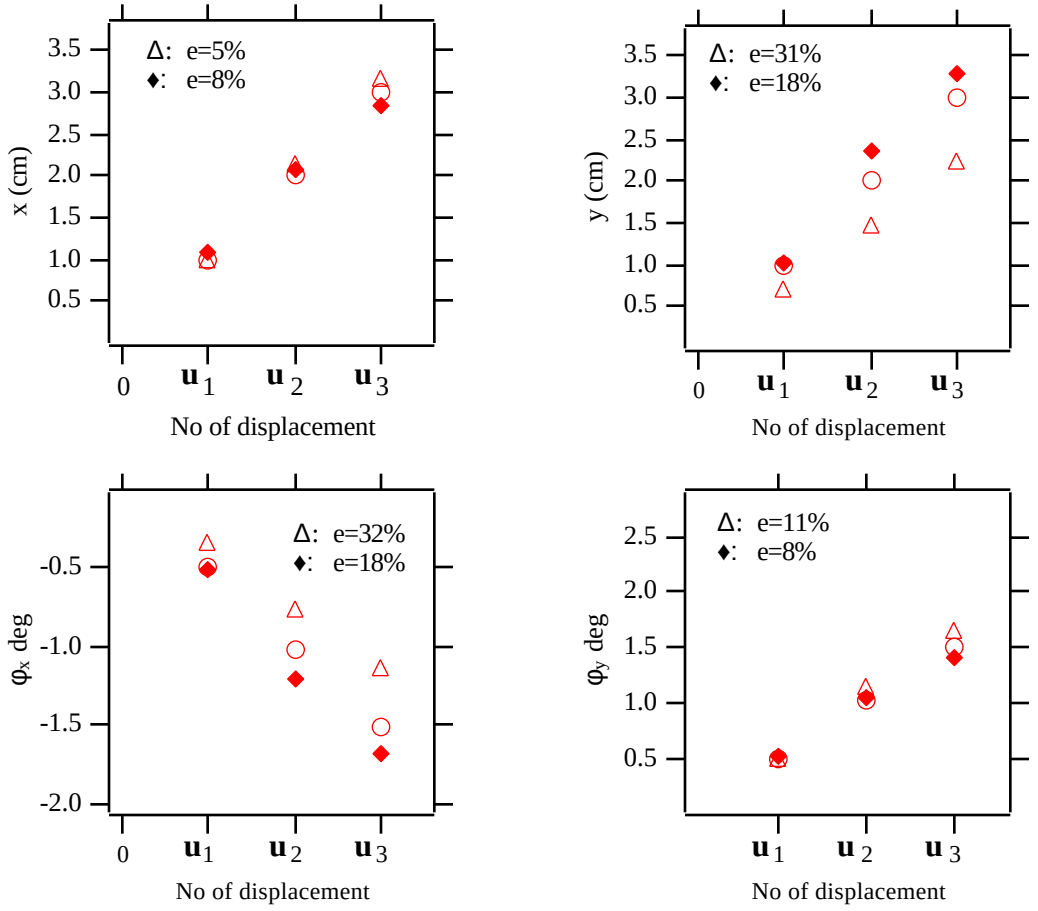

Figure 11: Experimental tests of displacement estimation

These experimental results verify qualitatively the results from simulations and also the methodology to find optimal strain sensor locations on the structure. Quantitative comparison of the simulation and experimental results is not possible because the error introduced in simulations and in experiments is not the same. In experiments the error is due to calibration errors and to strain measurement errors.

5.3.2 Inferred End-Point Control experimental validation

The manipulator end-effector is commanded to track a cartesian space line trajectory as shown on Figure 12.

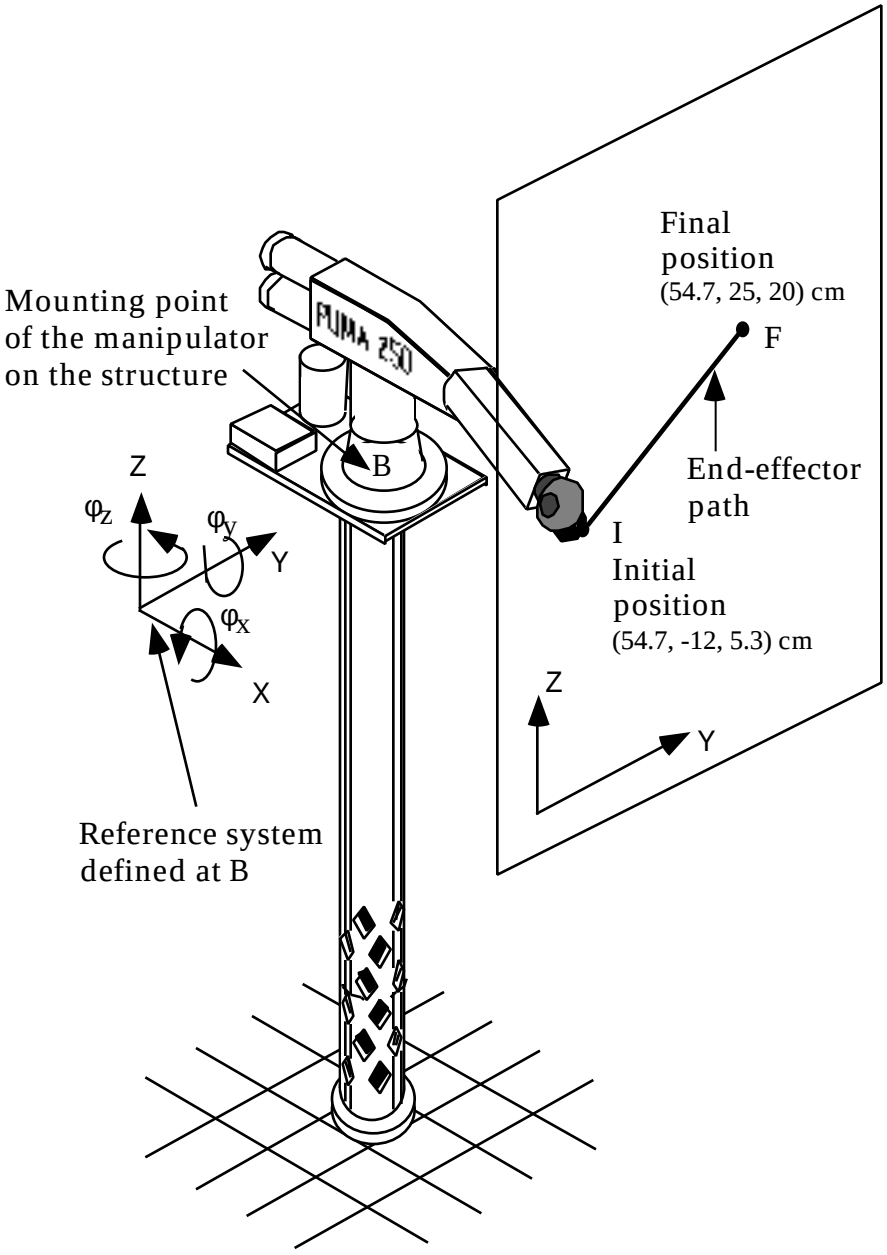

Figure 12: End-effector path

The commanded cartesian line lies on a plane parallel on the Z-Y plane of the reference system defined at point B. The reference system is defined as if the structure is undeformed under the

manipulator's weight. The coordinates of the initial and final points of the path expressed in the inertial reference system at B are shown on Figure 12 (points I and F on the Figure).

When the end-effector reaches its final position, the supporting structure is manually disturbed back and forth. The structure's motion during this combined path tracking and disturbance rejection test is shown on Figure 13. The base is disturbed a linear displacement of ±5cm in the x and ±7cm in the y direction and an angular displacement of ±3˚ around x and ±2˚ around y.

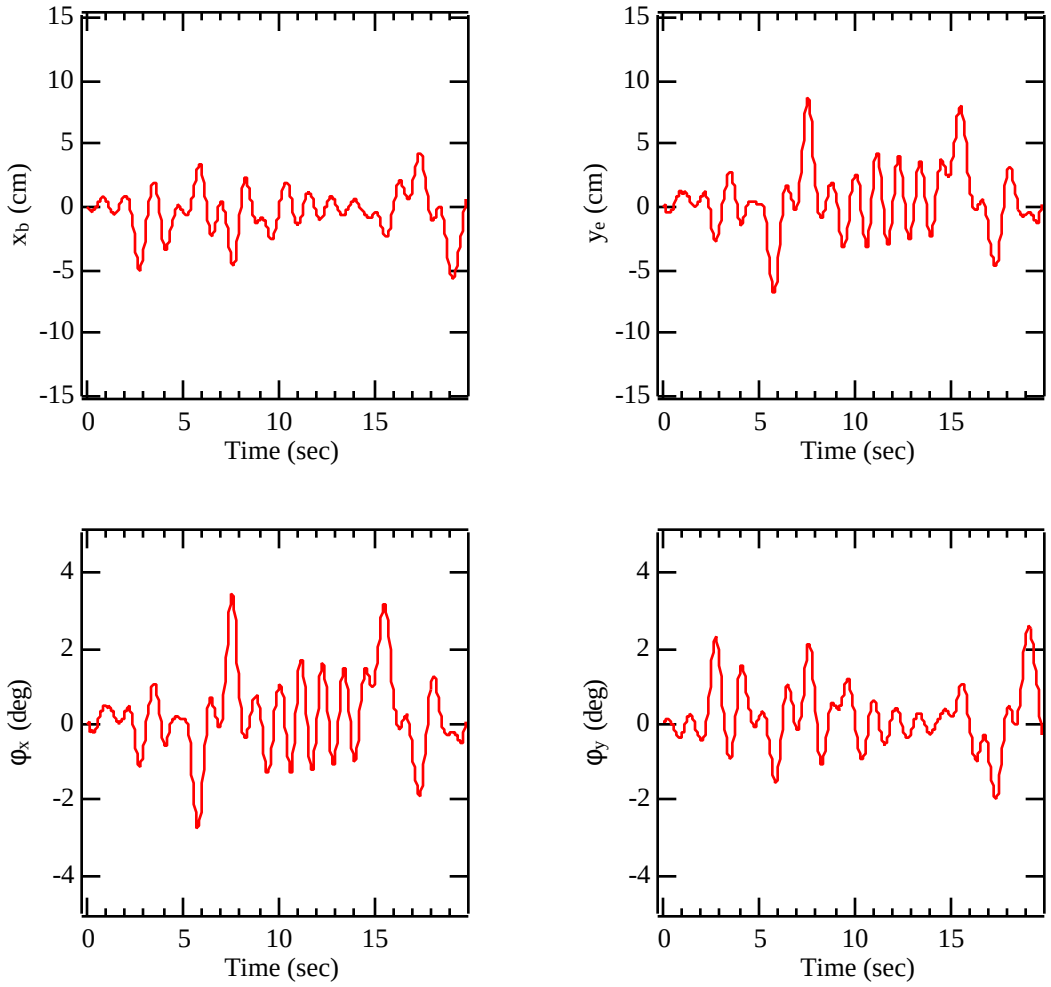

Figure 13: Motion of Shaky's structure

In spite of the substantial base motions the manipulator follows its commanded trajectory very closely and maintains this position with almost no oscillations (Figure 14.) With a conventional

PID joint controller the manipulator end-effector motion would be corrupted by the base motions, resulting in large end-effector errors (in the order of ±5cm.)

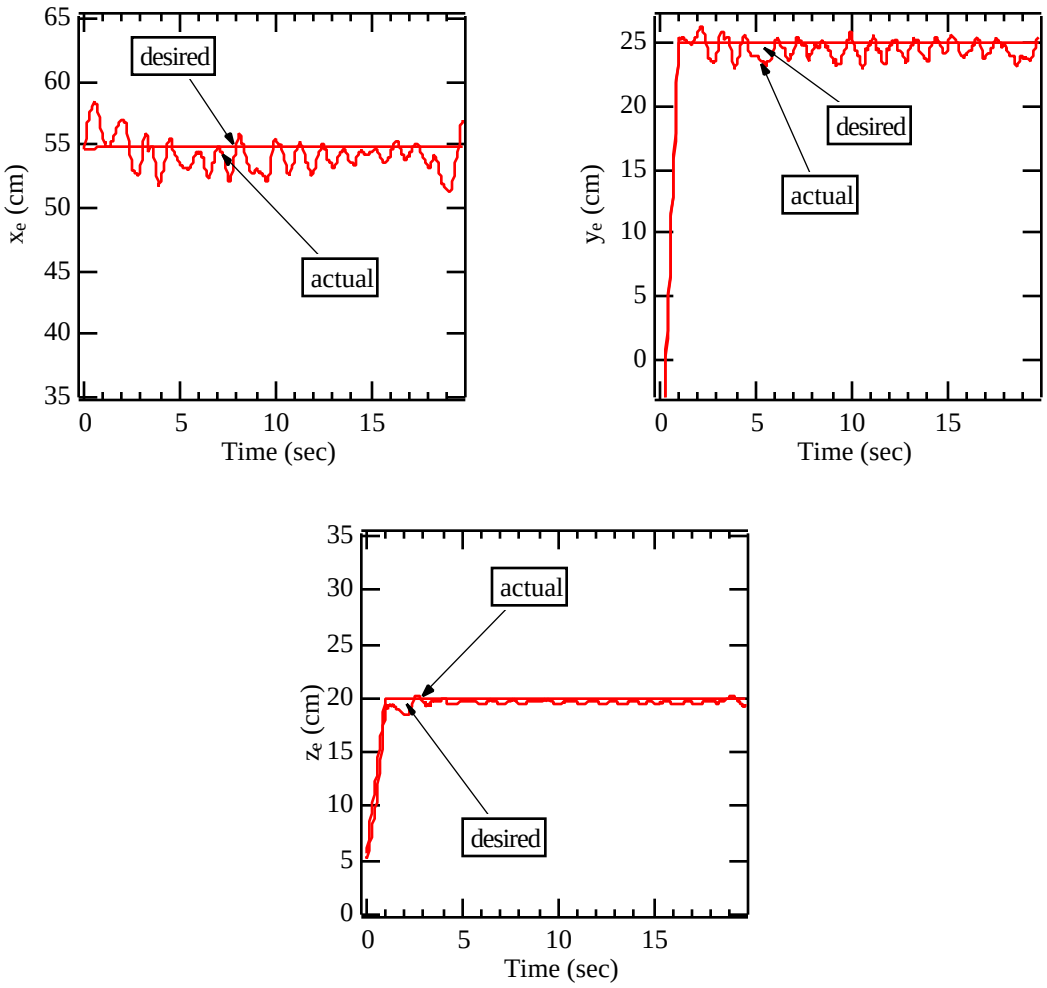

Figure 14: Manipulator end-effector coordinates

6. CONCLUSIONS

A method to optimally locate strain sensors on the flexible supporting structure of long reach manipulator systems has been presented. These strain measurements and a linear static strain-displacement model are used to estimate the flexible structure's motion. The criteria used to optimally place the strain sensors are: high measurement resolution, maximization of the distance from singular locations and minimization of the error in the identification of the strain-displacement model. Knowing the structure's motion and measuring the manipulator joint angles the

manipulator end-effector position and orientation in inertial system is calculated. This end-effector position/orientation measurement is used in an endpoint control scheme for long reach manipulators called Inferred End-point Control. The method for optimally placing strain sensors and the Inferred End-Point Control are validated on a six degree of freedom laboratory LRMS called Shaky II. This method for optimally measuring the motion of flexible structures can not only be used in the end-effector control of long reach manipulator systems but in the control of flexible manipulators as well.

7. ACKNOWLEDGMENTS

The support of this work by NASA Langley Research Center Automation Branch, Grant NAG 1-801 is acknowledged.

8. REFERENCES

1. Soler R. and Guillet J., "Robotic Maintenance of the EDF Transmission (63 to 400 KV) Network: Feasability Study and Effects on Tower Design," *Proceedings of the 6th International Conference on Transmission and Distribution Construction and Live Line Maintenance (ESMO '93)*, Las Vegas, NV, 1993, pp. 459-468.

2. Gibbons P. W. and McDaniel L. B., "First Generation Long Reach Manipulator for Retrieval of Waste from Hanford Single-Shell Tanks," Proceedings of the 6th ANS Topical Meeting on Robotics and Remote Systems, Monterey, CA, 1995.

3. Mori H., Iwata T. and Oda M., "An Overview of Japan's Space Automation and Robotics Activities," *Proceedings of the 1992 Artificial Intelligence, Robotics and Automation in Space (i-SAIRAS 92)*, Toulouse, France, 1992, pp. 19-24.

4. Dubowsky S., "Dealing With Vibrations in the Deployment Structures of Space Robotic Systems," *Proceedings of the 5th International Conference on Adaptive Structures*, Sendai, Japan, 1994.

5. Torres M.A., Dubowsky, S., and Pisoni, A., "Path-Planning for Elastically Mounted Space Manipulators: Experimental Evaluation of the Coupling Map," *Proceedings of the 1994 IEEE International Conference on Robotics and Automation*, San Diego, CA, 1994, pp. 2227-2233.

6. Lew J. and Book W., "Bracing Micro/Macro Manipulators Control," *Proceedings of the 1994 IEEE International Conference on Robotics and Automation*, San Diego, CA, pp. 2362-2368, 1994.

7. Torres, M.A. and Dubowsky S., "Pseudo-Passive Energy Dissipation," Proceedings of the 1995.

8. Trudnowski D.J., Baker C.P. and Evans M.S., "Damping Control of a Large Flexible Manipulator Through Inertial Forces of a Small Manipulator," *Proceedings of the American Control Conference,* San Fransisco, CA, pp. 2878-2879, 1993.

9. Lew J., Trudnowski D., Evans M. amd Bennett D., "Micro-Manipulator Motion Control to Counteract Macro Manipulator Structural Vibrations," *Proceedings of the 6th ANS Topical Meeting, Robotics and Remote Systems,* Monterey CA, 1995, pp. 487-491.

10. Sharon A. and Hardt D., "Enhancement of Robot Accuracy Using End-Point Feedback and a Macro-Micro Manipulator System," *Proceedings of the 1984 American Control Conference,* San Diego, CA, 1984, pp. 1836-1842.

11. Chiang, W., Kraft R. and Cannon R. "Design and Experimental Demonstration of Rapid, Precise End-Point Control of a Wrist Carried by a Very Flexible Manipulator," *The International Journal of Robotics Research,* 10, 1, 30-40, 1991.

12. Ballhaus W.L. and Rock S.M., "End-Point Control of a Two-Link Flexible Robotic Manipulator with a Mini-Manipulator: Coupling Issues," *ASME, AMD-Vol. 141/DSC-Vol. 37, Dynamics of Flexible Multibody Systems: Theory and Experiments,* 1992, pp. 17-22.

13. Hootsmans N. and Dubowsky S., "Large Motion Control of Mobile Manipulators Including Vehicle Suspension Characteristics," *Proceedings of the 1991 IEEE International Conference on Robotics and Automation,* Sacramento, Ca, April, 1991, pp. 2336-2341.

14. Chalhoub N. and Zhang X., "Reduction of the End-Effector Sensitivity to the Structural Deflection of a Single Flexible Link: Theoretical and Experimental Results," *Transactions of the ASME, Journal of Dynamic Systems, Measurement and Control,* 115, 658-666, 1993.

15. Vaillancourt C. and Gosselin, G., "Compensating for the Structural Flexibility of the SSRMS with the SPDM," *Proceedings of the International Advanced Robotics Program, Second Workshop on Robotics in Space,* Canadian Space Agency, Montreal, Canada, July, 1994.

16. Mavroidis C., Rowe P. and Dubowsky S., "Inferred Endpoint Control of Long Reach Manipulator Systems," *Proceedings of the International Conference on Intelligent Robots,* IROS 95, Pittsburg, PA, August 1995.

17. Magnami P. G. and S. M. Joshi, "Sensor Actuator Placement for Flexible Space Structures," *IEEE Transactions on Aerospace and Electronic Systems,* 29, 2, 1993, pp. 345-351.

18. Hac A. and Liu L., "Sensor and Actuator Location in Motion Control of Flexible Structures," *Journal of Sound and Vibration,* 167, 2, 1993, pp. 239-261.

19. Udwadia F., "Methodology for Optimum Sensor Locations for Parameter Identification in Dynamic Systems," *Journal of Engineering Mechanics,* 120, 2, 1994.

20. Zhang H., "Two Dimensional Optimal Sensor Placement," *IEEE Transactions on Systems Man and Cybernetics,* 25, 5, 1995.

21. Nakamura Y., "Geometric Fusion: Minimizing Uncertainty Ellipsoid Volumes," *Data Fusion in Robotics and Machine Intelligence,* M.A. Abidi and R. C. Gonzales, Eds. NY, 1992, pp. 457-479.

22. Bathe K. J. and Wilson E. L., *Numerical Methods in Finite Element Analysis*, Prentice Hall Inc., New Jersey, 1976.

23. Strang G., *Linear Algebra and Its Applications*, Harcourt Brace Jovanovich, Inc, San Diego, 1988.

24. Golub G. H. and Van Loan C. F., *Matrix Computations*, 2nd Edition (John Hopkins University Press, Baltimore, MD, 1989.

25. Klema V. and Laub A., "The Singular Value Decimposition: Its Computation and Some Applications," *IEEE Transactions on Automatic Control*, Vol. AC-25, No 2, 1980, pp 164-176.

26. Wilkinson J. H., *Rounding Errors in Algeberaic Processes*, Englewood Cliffs, NJ: Prentice Hall, 1963.

27. The Math Works Inc., *Matlab: High-Performance Numeric Computation and Visualization Software*, Natick, MA, October 1993.

28. Craig J., *Introduction to Robotics, Mechanics and Control*, Addison Wesley Publishing Company, Reading MA, 1989.

29. Hogan N., "Impedance Control: An Approach to Manipulation," *Transactions of the ASME, Journal of Dynamic Systems, Measurement and Control,* **107**, 1-24, 1985.

30. Khatib O., "A Unified Approach for Motion and Force Control of Robot Manipulators: The Operational Space Formulation," *IEEE Journal of Robotics and Automation,* **3**, 1, 43-53, 1987.

31. Dubowsky S. and Papadopoulos E., "The Kinematics, Dynamics, and Control of Free-Flying and Free-Floating Space Robotic Systems," *IEEE Transactions on Robotics and Automation,* **9**, 5, 531-543, 1993.

32. Hootsmans N. and Dubowsky S., "Large Motion Control of Mobile Manipulators Including Vehicle Suspension Characteristics," *Proceedings of the 1991 IEEE International Conference on Robotics and Automation*, Sacramento, Ca, April, 1991, pp. 2336-2341.

33. Thomas K., *Design of the Supporting Structure for a Laboratory Long Reach Manipulator System Using Finite Element Analysis*, Batchelor Thesis, Department of Mechanical Engineering, MIT, 1995.

34. ADINA R&D, Inc., *Automatic Dynamic Incremental Nonlinear Analysis*, Watertown, MA, September 1990.